Maximizing the Efficiency of Wireless Power Transfer Systems with an Optimal Duty Cycle Operation

Seyit Ahmet Sis[a], Hakan Akca*[b]

[a]*seyit.sis@balikesir.edu.tr, Balikesir University, Balikesir, Turkey*
[b]*hakca@gelisim.edu.tr, Istanbul Gelisim University, Istanbul, Turkey*

Abstract

In a typical high-power inductive wireless power transfer (WPT) system, AC signal, which drives the coupled resonant inductors (couplers), is produced by a half- or full-bridge inverter. However, the output voltage of an inverter is not a pure sinusoidal but a square wave with quite a few harmonics. Harmonics are expected to reduce active power transfer efficiency (APTE) due to high reactive power accumulation at the input to the resonant couplers. In this paper, WPT system efficiency is analyzed by introducing the harmonics of the voltage waveform of a typical inverter circuit in to an analytical model of the WPT system for the first time. In this regard, total harmonic distortion (THD) and harmonic content of the waveform, as well as the APTE of the system are all simulated as a function of duty cycle using an analytic model. Simulation results show that the THD of the source voltage waveform can be minimized with a duty cycle of 75%. Hence the reactive power at the input of the system is also minimized, increasing the APTE of the system in this duty cycle. An experimental wireless power transfer system is implemented to verify the aforementioned simulation based observation. The measured APTE is increased to a maximum of 94.5% from approximately 88.5% by simply reducing the duty cycle from 100% to 75%. The output power delivered to the load, on the other hand, decreases with this reduction in the duty cycle, if DC bus voltage stays constant. This trade of between efficiency and the delivered power to the load is analyzed in two wireless charging scenarios with different power and efficiency levels. We believe that the findings reported in this work would potentially lead researchers develop novel inverter structures to not only use for increasing power but also the efficiency of WPT systems.

Keywords: Wireless power transfer; duty cycle; inverter; active power

transfer efficiency; total harmonic distortion.

1. Introduction

Recent developments in magnetic coupling based wireless power transfer (WPT) systems are quite appealing to many industrial, consumer and military applications. Eliminating power cords reduces the risk of electric shock and makes power transfer more practical than wired chargers. Static and possibly dynamic wireless charging of electric vehicles (EVs) will potentially accelerate the use of EVs, which is essential for reducing carbon emission [1, 2, 3, 4]. Wirelessly powering industrial machines and robots, charging mobile electronic devices and other consumer electronics have similar advantages of being more practical and less risky for occupational and home accidents. Such a large number of potential applications pave the way for WPT systems with different power levels and operation frequencies. For example, low power WPT systems, specifically the ones adopting Alliance for Wireless Power (A for WP) standard, operates at high frequency (HF) band (e.g 6.78 MHz) [5]. The HF power is produced from an RF power source, usually a high efficiency Class-E RF power amplifier [6, 7, 8, 9]. RF power sources exhibit a 50Ω or 75Ω source resistance and provides a pure sinusoidal signal to the system. From an RF engineer's point of view, efficiency is defined as the power delivered to the load to the power available from the source [10, 11, 12, 13]. One can obtain efficiency response, extract all the resonance frequencies and observe so called frequency-splitting phenomenon by simply measuring the 2-port network parameters (e.g. S-parameters) of the coupled resonance coils [10, 14].

On the other hand, for high power WPT systems (e.g EV chargers), bridge type inverters are the most practical and cost efficient solution to produce required power levels (e.g Pout> 1 kW). Switching frequency of these inverters is limited to several hundred kHz, restricting the maximum operation frequencies of high power WPT systems up to 150 kHz [15, 16, 17, 18]. For these type of inverter-driven WPT systems, APTE can be defined as the power delivered to the load to the apparent power at the output of the inverter [19, 20]. Fig. 1 shows a general circuit model for an inverter driven WPT system with a series-series (SS) compensation topology. Unlike RF power sources, inverters produce a periodic square wave with quite a few harmonics.
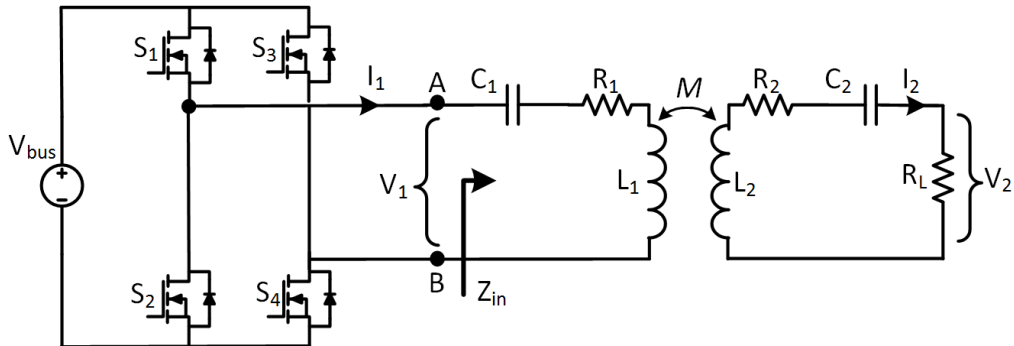
2

Figure 1: A circuit model for an inverter-driven WPT system with a series-series (SS) compensation topology.

If we consider the efficiency response for a WPT system as a band-pass filter response, harmonics' frequencies of the input voltage waveform are beyond this pass band. The input impedance at the harmonics' frequencies, therefore, is predominantly reactive and reduces the APTE.

Several works, related to analysis of harmonics content of the inverter signal in WPT systems, are reported in the literature [21, 22, 23, 24, 25]. In [21], authors aimed at eliminating the harmonics at the current waveform using an LC low-pass filter, but system efficiency is not investigated in detail. In [22], a class-E rectifier is proposed for use in a MHz range WPT system. The authors report that the input voltage THD of the Class E full-wave rectifier is reduced to one fourth of the THD of a conventional full-bridge rectifier [22]. However, this analysis is limited to the rectifier only. Reactive power levels are compared in WPT systems with different compensation schemes in [23]. A simple conclusion comes out that the LCC compensation circuit has the minimum reactive power among different various compared schemes [23]. Cascaded multi-level inverter is proposed for high power WPT systems in [24, 25]. The authors utilize the multi-level inverter primarily for increasing the power level of the inverter and partially discuss about selective harmonic elimination. However; relationship between system efficiency and harmonic content of the inverter voltage is not analyzed in these publications [24, 25].

1.1. Contribution

In this work, we analyze an inverter-driven WPT system with the aim of understanding the effect of harmonic content on the APTE. Harmonic con-

3

tent and total harmonic distortion (THD) of a symmetric square waveform, which is what an inverter produces, are calculated as a function of duty cycle. At the same time, the input and the output power, and the APTE of the system are simulated as a function of duty cycle. Simulation results show that the THD of the input voltage is minimum with an optimal duty cycle of approximately 75%. Therefore, the reactive power accumulation at the input to the primary side coupler is also minimum at this duty cycle. Using analytic expressions derived from a WPT circuit model, the APTE, which is defined as the ratio of power delivered to the load to the apparent power at the input to the coupled inductors (couplers), is shown to be maximized by simply operating the inverter with an approximately 75% duty cycle. These simulation based results are finally verified in an experimental WPT system.

Increasing the APTE to near 100% is one of the major goals for researchers working on WPT systems. Most of the works so far have been on designing novel coil structures with low power loss and high coupling coefficients [26, 27, 28, 29, 30, 31, 32, 33]. The findings in this piece of work, on the other hand, recommend one to operate the inverter at an optimal duty cycle of 75% if maximum efficiency is targeted. The originality of this paper comes from the fact that the relationship between inverter signal's harmonic content and WPT system efficiency is reported and experimentally verified in such detail for the first time. We believe that the findings reported in this work would potentially lead researchers to develop novel inverter structures to not only use for increasing power but also the efficiency of WPT systems by considering the effect of harmonics on the power transfer efficiency.

2. Modeling and Efficiency Response For An Inverter-Driven WPT System

The circuit model shown in Fig.1 utilize a full-bridge inverter consisting of four MOSFET switches, represented by S_1, S_2, S_3 and S_4. This inverter is controlled by a phase shifted pulse width modulation (PSPWM) algorithm of which signal diagram is shown in Fig.2. The signals at the gates of the S_1, S_2, S_3 and S_4 switches are symbolized with G_{S1}, G_{S2}, G_{S3} and G_{S4}, respectively. The S_1-S_2 and S_3-S_4 switches are driven with complementary gate signals. As seen in the signal diagram, duty cycle variation is realized by providing time delays between driving signals of S_1 and S_4 as well as S_2 and S_3. The output voltage signal of an inverter is shown as V_{AB} in this

4

figure. The total pulse width and the period of the signal are represented with τ and T, respectively.
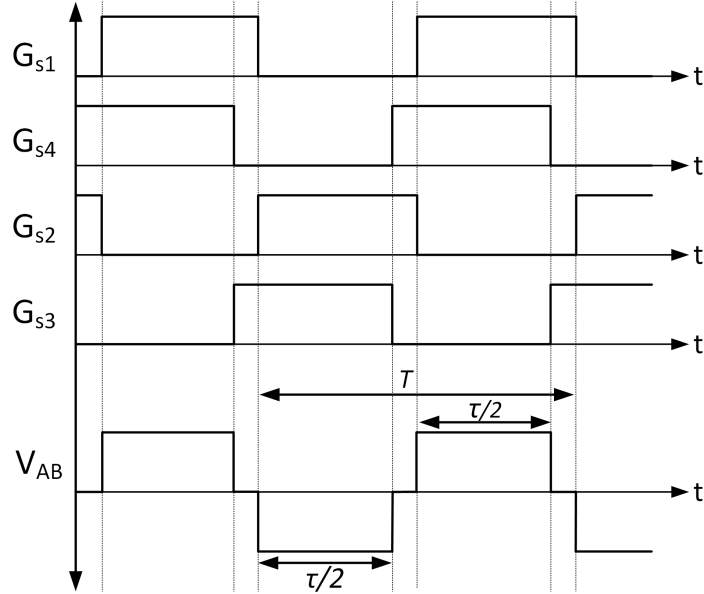

Figure 2: Signal diagram for PSPWM.

The switches are fed from a DC bus and each switch has an on state resistance (R_{dson}) between drain-source terminals. Since two pair of transistors (S_1-S_3 and S_2-S_4), are switched on/off successively, and at any instant of time only one pair is on while the other is off, the model in Fig.1 can be simplified to the one as shown Fig.3. The DC bus voltage (V_{bus}), shown in Fig.1, becomes the peak value of the square wave voltage source shown in Fig.3.

In Fig.3, magnetically coupled primary and secondary side couplers are represented with two inductors, L_1 and L_2, which are coupled through a mutual inductance of M. The series connected compensation capacitors are represented with C_1 and C_2. The losses of coils, mainly originated from the AC resistance of wires, is modeled via R_1 and R_2. The load resistance is modeled with R_L in this circuit model. The input voltage is a symmetric square waveform (see Fig.2) of which amplitude is ideally equal to the DC bus voltage, hence is represented by V_{bus}. In the following sub-section (section
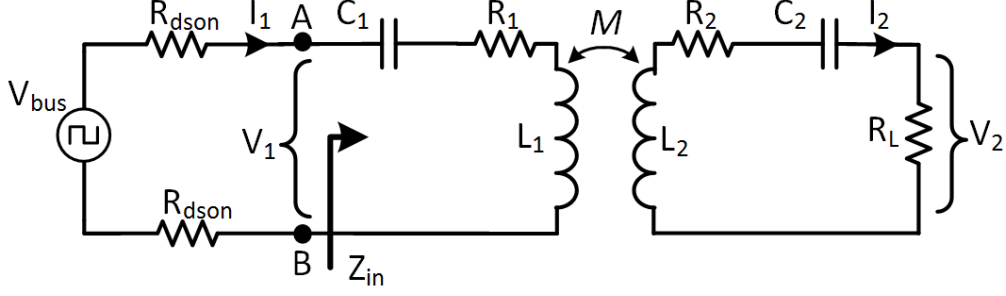
5

Figure 3: A more simplified circuit model for an inverter-driven WPT system.

2.1), we analyze the inverter's output voltage which is essentially a non-sinusoidal waveform.

2.1. Harmonic Analysis of Source Voltage

The symmetric square wave can be expressed with fourier series expansion as follows:

$$V_{bus}(t) = a_0 + \sum_{k=0}^{\infty} a_k \cos(k\omega_0 t) \tag{1}$$

where $\omega_0(2\pi/T_0)$ and k are the fundamental radial frequency of the signal and harmonic indice, respectively. The zeroth harmonic, a_0, is the DC component and is equal to zero for a square wave with a symmetry along time axis (see Fig. 2). Amplitudes of higher harmonics, a_k, for a symmetric square wave can be expressed as a function of duty cycle $(d=\tau/T)$ and peak-to-peak voltage $(V_{bus_{pk-pk}})$ as follows:

$$a_k = \frac{2V_{bus_{pk-pk}}}{k\pi} \sin\left(\frac{k\pi d}{2}\right) \tag{2}$$

Using the amplitude of each harmonic in (2), the total harmonic distortion (THD) for a symmetric square wave signal can be calculated as follows [34]:

$$THD = \frac{\sqrt{a_3^2 + a_5^2 + \ldots + a_n^2}}{a_1}. \tag{3}$$

The normalized peak values for each harmonic of a symmetric square wave is calculated as a function of duty cycle using (2) and shown in Fig.4.

6

As seen in Fig.4, the first harmonic (fundamental) is the dominant one and its amplitude constantly increases with the duty cycle. The THD is mainly increased by the third and the fifth harmonics; however, up to ninth harmonics are calculated using (3) and utilized in the calculation of the THD. It should be noted that all the even harmonics are zero for this symmetric square waveform.
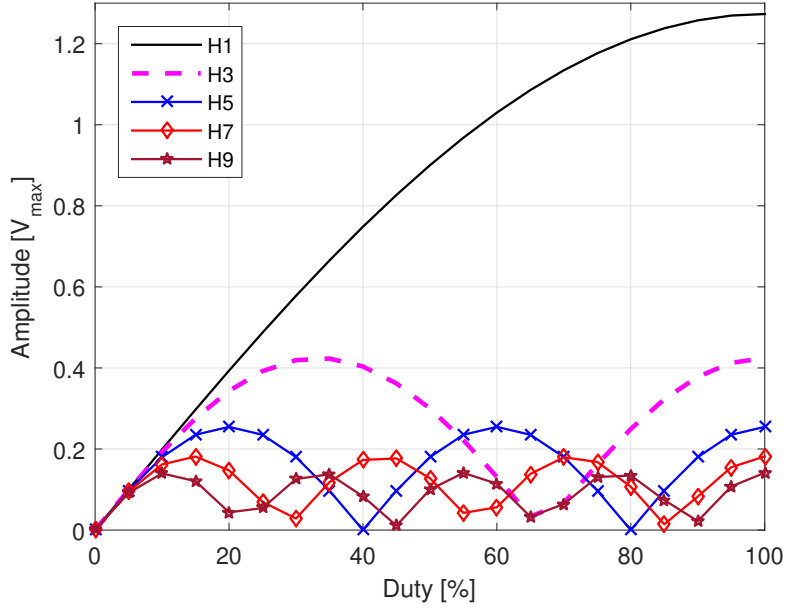

Figure 4: The normalized peak values, as a function of duty cycle.

Fig.5 shows calculated THD as a function of duty cycle for a symmetric square wave. The THD exhibits its minimum value of approximately 27% when the duty cycle 75%. That is, the overall harmonic content of a symmetric square wave is minimum with this duty cycle. If we consider the efficiency response of a WPT system as a band-pass filter response, harmonics' frequencies are beyond this pass band and the input impedance at these harmonic frequencies is predominantly reactive. Minimum THD means minimum harmonic-related reactive power; therefore, the apparent power level becomes closer to the active power level at the input to the couplers. It is for this reason that one can expect maximum active power transfer efficiency (APTE) at the 75% duty cycle. A mathematical expression for the efficiency can be obtained from the current and voltage expressions at the in-
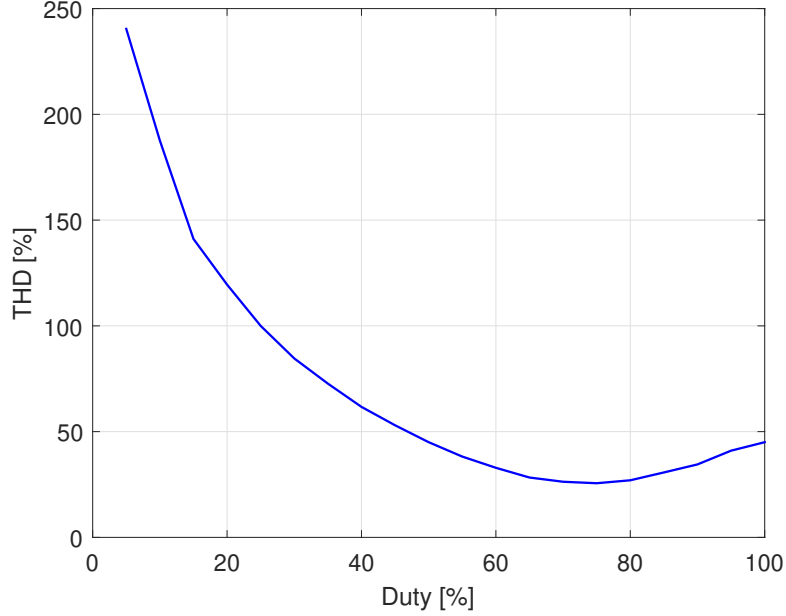
7

Figure 5: THD vs duty cycle for the symmetric square wave.

put and output of the system. The simplified lumped element model, shown in Fig.3 can be utilized for this purpose as will be discussed in the following sub-section.

2.2. Efficiency Response

The WPT system, as modeled in Fig.3, can be assumed to be linear and the response of a linear time-invariant (LTI) system to any input consisting of a linear combination of sinusoidal signals is the same linear combination of the individual responses to each of the sinusoidal signal [35]. Therefore, by analyzing the model in Fig.3, one can express the current flowing through the load resistance (I_{2_k}) due to each harmonic of the input voltage, a_k as shown in (4).

$$I_{2_k} = \frac{jk\omega a_k}{\left(R_1 + 2R_{dson} + jk\omega L_1 - \frac{j}{k\omega C_1}\right)\left(R_L + k\omega L_2 - \frac{j}{k\omega C_2}\right) + (k\omega M)^2}. \quad (4)$$

The root mean square (rms) of the load current ($I_{2_{rms}}$) is calculated using its components at each harmonic (I_{2_k}) as;

$$I_{2_{rms}} = \sqrt{\frac{I_{2_1}^2 + I_{2_3}^2 + \ldots + I_{2_n}^2}{2}}. \tag{5}$$

The power delivered to the load (P_L) is calculated using the load current and the load resistance as follows:

$$P_L = |I_{2_{rms}}|^2 R_L. \tag{6}$$

At the primary side, the input impedance seen towards the resonant primary side coil at kth harmonic, Z_{in_k}, can be extracted from the circuit model as follows:

$$Z_{in_k} = R_1 + j\left(k\omega L_1 - \frac{1}{k\omega C}\right) + \frac{(k\omega M)^2}{R_2 + R_L + j\left(k\omega L_2 - \frac{1}{k\omega C_2}\right)}. \tag{7}$$

Subsequently, at each harmonic, the input current flowing through primary side resonant coil can be expressed as:

$$I_{1_k} = \frac{a_k}{Z_{in_k}}. \tag{8}$$

The rms of the input current is then calculated using its harmonic content from (8) as folllows:

$$I_{1_{rms}} = \sqrt{\frac{I_{1_1}^2 + I_{1_3}^2 + \ldots + I_{1_n}^2}{2}}. \tag{9}$$

The input voltage seen at the input of the resonant primary side coupler, for each harmonic, can be calculated by subtracting the voltage drop across the two series R_{dson} resistances (see Fig.3) from the harmonics of V_{bus} as given below.

$$V_{1_k} = a_k - 2I_{1_k}R_{dson}. \tag{10}$$

The rms of input voltage is then calculated as follows:

$$V_{1_{rms}} = \sqrt{\frac{V_{1_1}^2 + V_{1_3}^2 + \ldots + V_{1_n}^2}{2}}. \tag{11}$$

9

By using the RMS values of voltage and current at the input to the primary side coupler, V_1 and I_1, the apparent power at the input (S_{in}) can be calculated as follows:

$$S_{in} = V_{1_{rms}} I_{1_{rms}}. \tag{12}$$

Finally, the APTE of the WPT system can be calculated by using the (P_L) and (S_{in}) in (6) and (12) as follows:

$$APTE = \frac{P_L}{S_{in}}. \tag{13}$$

Using the analytic model given in (4)-(13), the efficiency of the WPT system is simulated as a function of frequency for various duty cycles. In these simulations, inductance and resistance values (L_1, L_2, M and R) are obtained from the LCR meter measurements of fabricated coils utilized in the experiments. All the component values utilized in simulations are listed in Table 1. Fig.6 shows simulated APTE as a function of frequency for duty cycles of 55%, 75%, 90% and 100%. As seen in this figure, for all duty cycles, WPT system exhibits three peaks at approximately 25 kHz, 28 kHz and 33 kHz, respectively. These frequencies are the resonance frequencies of the coupled resonator system. Fig. 6 shows that the APTE exhibits its highest response when duty cycle is 75%. This is attributed to the fact that if the THD of the source voltage is minimum, harmonic-related reactive power is also minimum, making apparent power level closer to the active power level. To better observe the effect of duty cycle, the APTE is also simulated as a function of duty cycle at the resonance frequencies, 25 kHz, 28 kHz and 33 kHz. Fig.7 shows simulated peak APTE values as a function of duty cycle at these resonance frequencies. This figure agrees with Fig. 6 such that maximum efficiency for all the resonance frequencies are observed at 75% duty cycle as well. Next section presents an experimental WPT system that verifies the simulation results discussed so far and elaborate the trade off between efficiency and power delivered to the load.

3. Experimental Setup and Measurement Results

An experimental WPT system is set up as shown in Fig. 8a. The experimental setup employs a full-bridge inverter, coupled inductors (couplers) with series-series (SS) compensation capacitors and a load resistance (R_L) of

Table 1: Characteristic values of the simulated WPT system

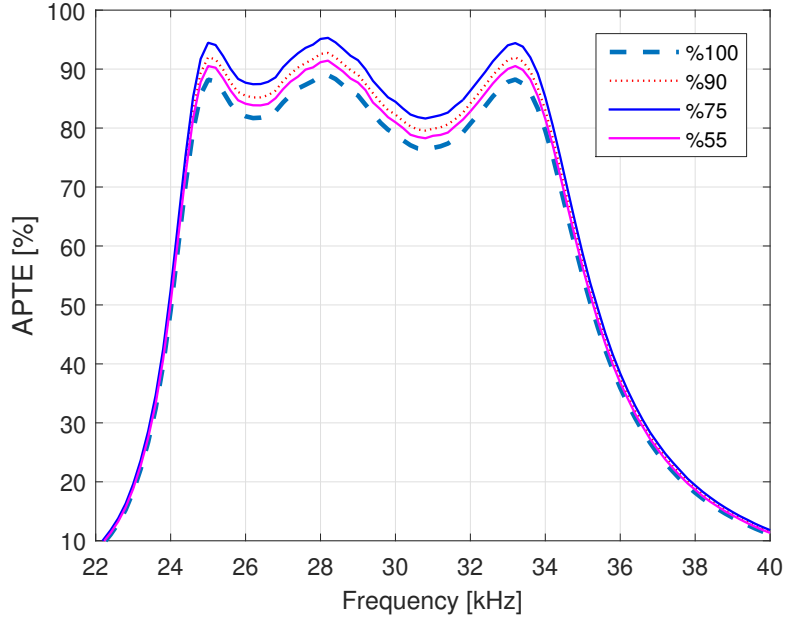| Components	L_1, L_2	M	C_1, C_2	R_1, R_2
Values	$182\mu H$	$57\mu H$	$176nF$	$29m\Omega$

Figure 6: Simulated APTE response for duty cycles of 55%, 75%, 90% and 100%.

5Ω. The inverter consists of four FQA30N40 MOSFET switches which are driven through their gates using TMDSDOCK28335 digital signal controller (DSC). The voltage and current data at the input and the output of the system is collected with an NI6356 data acquisition (DAQ) card. The input and the output voltages of the WPT system is measured by connecting the input and output nodes to this DAQ card. The currents, on the other hand, are measured through Textronix current probe and amplifier (TCP305). The DAQ card's sampling time is $1\mu s$ and the power calculations are performed instantaneously during the measurement. The couplers are fabricated based on compact flux-pipe structure exhibiting high coupling coefficient [27]. Flux-pipe couplers in this work employ three sub-coils which are wound around a
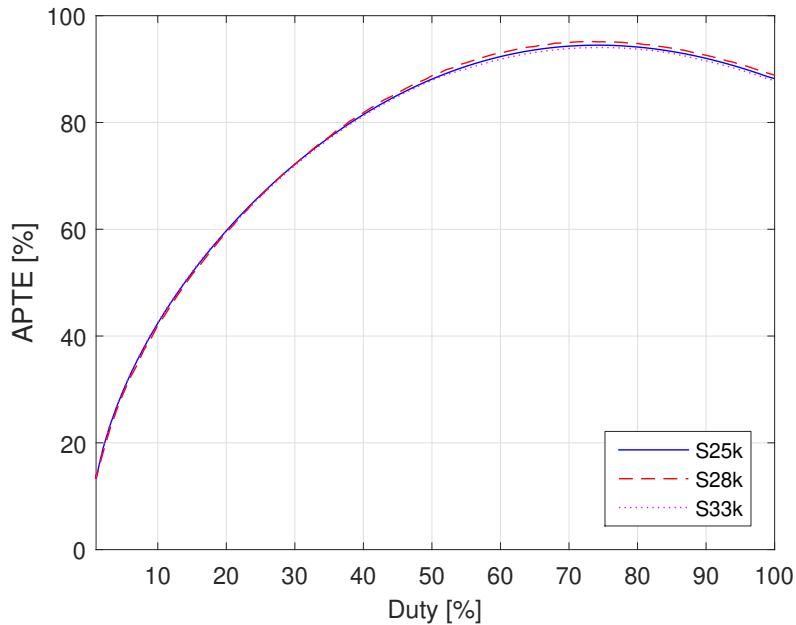
Figure 7: Peak efficiency vs duty cycle for all resonance frequencies.

common ferrite structure as seen in Fig.8b. The geometry of the couplers is designed for achieving maximum coupling coefficient (k_c) between them. The design details and simulation results for the couplers are beyond the scope of this paper and can be found elsewhere [36].

In experiments, first, efficiency response is measured and compared to that of simulation results for 75% duty cycle. As seen in Fig.9, simulation and measurement results agree very well, verifying the accuracy of the circuit model utilized in simulations. Subsequently, the efficiency response is measured for duty cycles of 55%, 90% and 100% ,as well, and compared to that of 75% duty cycle as shown in Fig.10. As seen in these measured data, maximum APTE is observed for the duty cycle of 75%, agreeing with the simulation results in Fig.6.

Measured peak efficiency values at approximately 25 kHz, 28 kHz and 33 kHz resonance frequencies, are plotted as a function of duty cycle as seen in Fig.11a. Again in this figure, maximum efficiency for all the resonance frequencies is observed at 75% duty cycle. The pictures in Fig.11b and Fig.11c are the oscilloscope screenshots and show the input and output voltage and current waveforms for 100% and 75% duty cycles, respectively.
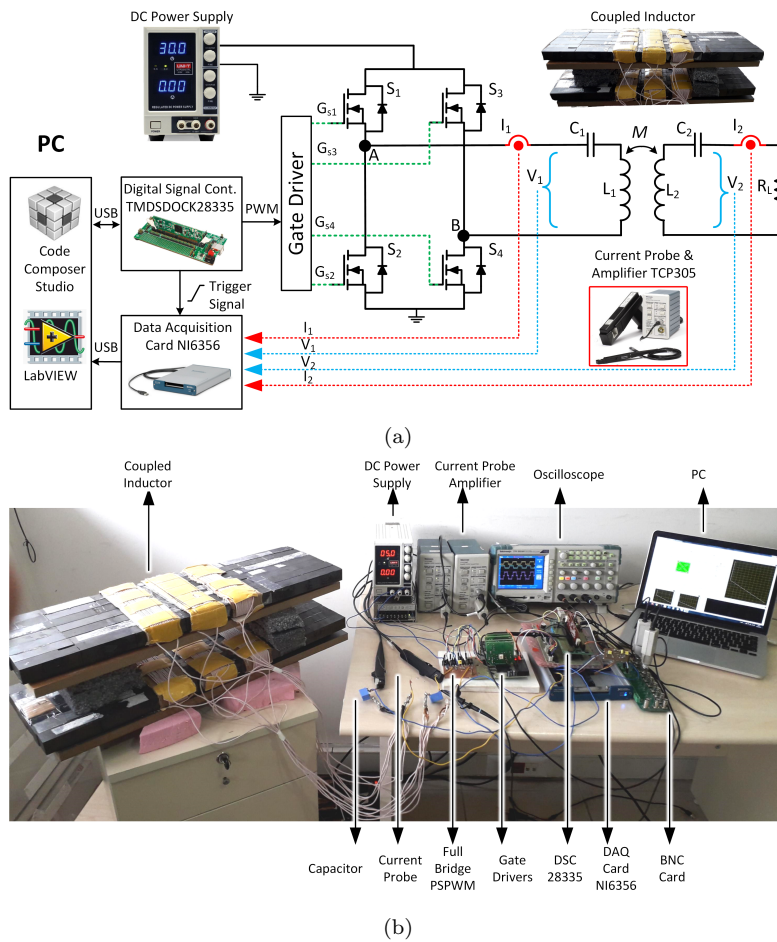
12

Figure 8: (a) Schematic and (b) photograph for an experimental WPT system.

In both Fig.11b and c, the input current and voltage waveforms are shown at the upper half of the oscilloscope screen, while the output voltage and current waveforms are shown at the bottom half of the screen. At 33 kHz, the voltages and currents are in-phase and in good shape verifying that 33 kHz is one of the resonance frequencies of the coupled system.

Both simulation and the experimental results show that one needs to operate the inverter with a 75% duty cycle for boosting active power transfer efficiency to its maximum level. This efficiency improvement, however, comes with the cost of a reduction in the power delivered to the load (P_L). To better visualize the trade off between the efficiency and the power delivered to the
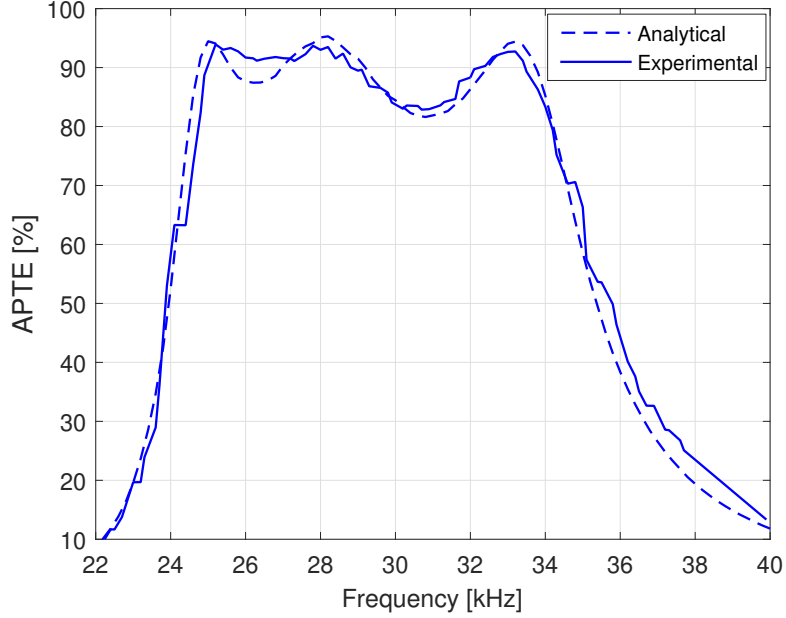
Figure 9: Simulated and measured frequency response of efficiency for 75% duty cycle.

load, both of them is plotted as a function of duty cycle on the same graph as seen in Fig. 12. The normalized P_L is increasing with the duty cycle persistently and reaches its maximum at a duty cycle of 100% (Fig. 12). At 75% duty cycle, where efficiency is maximum, the P_L is nearly 15% less than its maximum value at 100% cycle. Therefore, this decrease at the output power level would increase the charging time.

Table 2 shows a time-energy consumption analysis for a 3.3 kW charger utilizing the above presented WPT system. The analysis is performed for two different scenarios to charge a 16 kWh battery. In Scenario I, the WPT system is driven with an 100% duty cycle waveform (maximum power mode), and in Scenario II, the WPT system is driven with a 75% duty cycle waveform (maximum efficiency mode). As seen in Table 2, the battery is fully charged in 4.85 hours with a total energy consumption of 18.08 kWh in maximum power mode. In the maximum efficiency mode, the exact same battery is fully charged in 5.71 hours with less than 17 kWh energy consumption. Depending on the preferences (cost or time), either mode can be selected by the user.

Finally, the findings presented in this work are summarized in Table 3 along with the findings from similar works related to harmonic analysis in
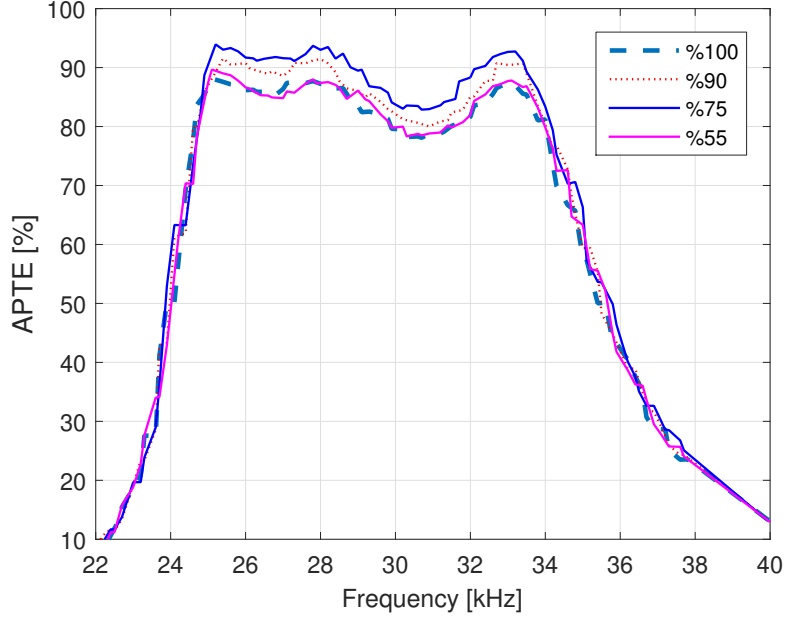
14

Figure 10: Measured frequency response of efficiency for various duty cycles.

Table 2: Time-energy consumption analysis for an example 3.3 kW WPT system to charge a 16 kWh battery. Two different charging scenarios are considered in the analysis

	Duty (%)	Pout (kW)	Efficiency (η)	Energy (kWh)	Time (h)
Scenario I (Max Power)	100	3.3	88.5	18.08	4.85
Scenario II (Max Eff.)	75	2.8	94.5	16.93	5.71

WPT systems reported in literature [21, 22, 23, 24, 25]. Each reported work has a different approach, goal and even operating frequency; therefore, Table 3 is not meant to provide a very direct comparison of the performance of reported WPT systems, but to clearly show the differences of this work in a comparative manner.
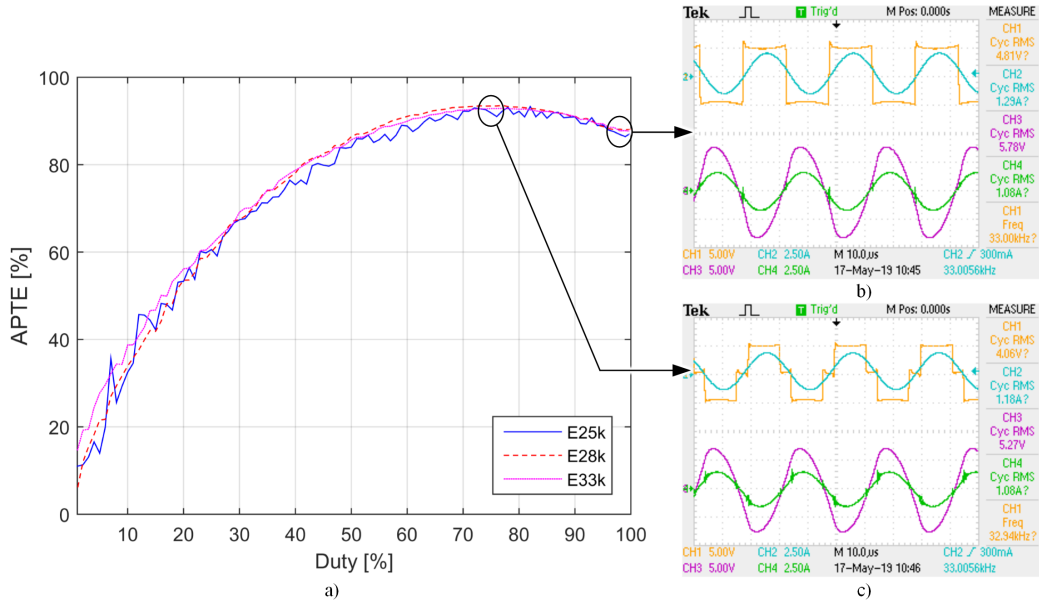
15

Figure 11: a) Peak efficiency values at resonance frequencies as a function duty cycle. Oscilloscope screenshots for the measurements at the 33 kHz resonance frequency b) 100% duty cycle c) 75% duty cycle

Table 3: Comparison of this work with similar works on the harmonic analysis in WPT systems reported in the literature.

Ref	Method	Control Side ($Primer or Seconder$)	THD ($V or I$)	Efficiency (η)	Frequency
[21]	Additional LC Filter after Inverter	Primer	THD$_I$<%5 Input current	>%90	20kHz
[22]	Class E rectifier after receiver coil	Seconder	THD$_V$=%9.9 Input of the Full wave rectifier	%80	6.78MHz
[23]	Reactive power minimization with LCC compensation	Both	NA	NA	85kHz
[24,25]	Utilization of cascaded and multilevel inverters	Primer	THD$_V$=%16-75	%87.5	20kHz
This Work	Duty-Cycle control	Primer	THD$_V$=%25	%94	25kHz or 33kHz

4. Conclusion

In this paper, WPT system's efficiency is analyzed by introducing the harmonics of the voltage waveform of a typical inverter circuit in to an analytical
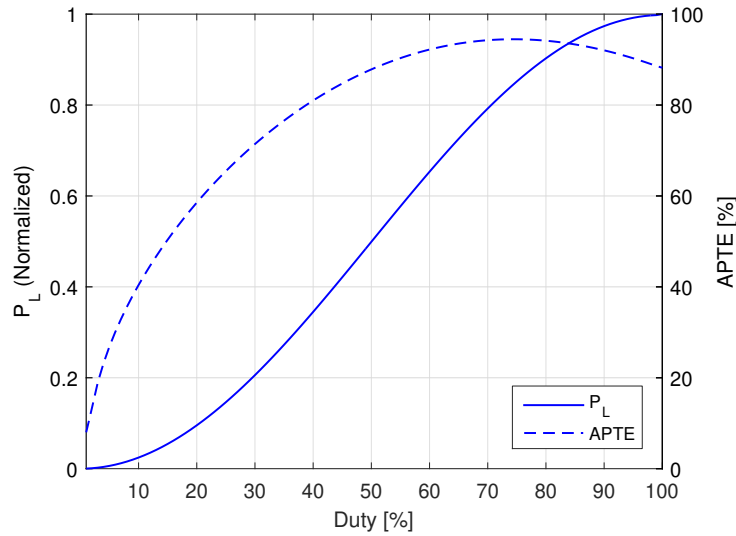
16

Figure 12: Active power transfer efficiency (APTE) and normalized power delivered to the load (P_L) as a function of duty cycle

model of the WPT system for the first time. We show that the efficiency response of an inverter-driven wireless power transfer system can be maximized by minimizing the harmonic-related reactive power accumulation at the input to the inductive couplers. The harmonic-related reactive power is minimized through operating the inverter with an optimal 75% duty cycle at which the THD of the source voltage becomes minimum. This efficiency maximization is explained by utilizing the Fourier series expansion of the voltage waveform and analytical model of the WPT system simultaneously. These theoretical observations are verified in an experimental wireless power transfer system with an excellent agreement. We believe that the findings reported in this work would potentially lead researchers to develop novel inverter structures to not only use for increasing power but also the efficiency of WPT systems by considering the effect of harmonics on the power transfer efficiency. Therefore, an important future direction of this work is to implement multistage inverter topologies to create waveforms with even lower harmonic content and realize WPT systems with even higher efficiencies.

References

[1] Z. Bi, L. Song, R. De Kleine, C. C. Mi, G. A. Keoleian, Plug-in vs. wireless charging: Life cycle energy and greenhouse gas emissions for an electric bus system, Applied Energy 146 (2015) 11–19. doi:10.1016/J.APENERGY.2015.02.031.
URL https://www.sciencedirect.com/science/article/pii/S0306261915002081

[2] Z. Bi, T. Kan, C. C. Mi, Y. Zhang, Z. Zhao, G. A. Keoleian, A review of wireless power transfer for electric vehicles: Prospects to enhance sustainable mobility, Applied Energy 179 (2016) 413–425. doi:10.1016/J.APENERGY.2016.07.003.
URL https://www.sciencedirect.com/science/article/pii/S0306261916309448

[3] S. Lukic, Z. Pantic, Cutting the Cord: Static and Dynamic Inductive Wireless Charging of Electric Vehicles, IEEE Electrification Magazine 1 (1) (2013) 57–64. doi:10.1109/MELE.2013.2273228.
URL http://ieeexplore.ieee.org/document/6648485/

[4] H. Humfrey, H. Sun, J. Jiang, Dynamic charging of electric vehicles integrating renewable energy: a multi-objective optimisation problem, IET Smart Grid (2019) 1–10doi:10.1049/iet-stg.2018.0066.

[5] J. Huang, Y. Zhou, Z. Ning, H. Gharavi, Wireless Power Transfer and Energy Harvesting: Current Status and Future Prospects, IEEE Wireless Communications (2019) 1–7doi:10.1109/MWC.2019.1800378.
URL https://ieeexplore.ieee.org/document/8715340/

[6] B.-C. Kim, B.-H. Lee, Class-E power amplifier with minimal standby power for wireless power transfer system, Vol. 13, 2018. doi:10.5370/JEET.2018.13.1.250.

[7] J.-R. Yang, J. Kim, Y.-J. Park, Class E Power Amplifiers using High-Q Inductors for Loosely Coupled Wireless Power Transfer System, Vol. 9, 2014. doi:10.5370/JEET.2014.9.2.569.

[8] P. S. Riehl, A. Satyamoorthy, H. Akram, Y.-C. Yen, J.-C. Yang, B. Juan, C.-M. Lee, F.-C. Lin, V. Muratov, W. Plumb, P. F. Tustin, Wireless Power Systems for Mobile Devices Supporting Inductive and Resonant

Operating Modes, IEEE Transactions on Microwave Theory and Techniques 63 (3) (2015) 780–790. doi:10.1109/TMTT.2015.2398413.
URL http://ieeexplore.ieee.org/document/7039275/

[9] M. Fu, H. Yin, M. Liu, C. Ma, Loading and Power Control for a High-Efficiency Class E PA-Driven Megahertz WPT System, IEEE Transactions on Industrial Electronics 63 (11) (2016) 6867–6876. doi:10.1109/TIE.2016.2582733.
URL http://ieeexplore.ieee.org/document/7496996/

[10] T. Imura, Y. Hori, Maximizing air gap and efficiency of magnetic resonant coupling for wireless power transfer using equivalent circuit and Neumann formula, IEEE Transactions on Industrial Electronics 58 (10) (2011) 4746–4752. doi:10.1109/TIE.2011.2112317.

[11] S. A. Sis, S. Kavut, A frequency-tuned magnetic resonance-based wireless power transfer system with near-constant efficiency up to 24 cm distance, Turkish Journal of Electrical Engineering and Computer Sciences 26 (6) (2018) 3168–3180. doi:10.3906/elk-1803-98.

[12] S. A. Sis, S. Bicakci, A resonance frequency tracker and source frequency tuner for inductively coupled wireless power transfer systems, in: 2016 46th European Microwave Conference (EuMC), IEEE, 2016, pp. 751–754. doi:10.1109/EuMC.2016.7824452.
URL http://ieeexplore.ieee.org/document/7824452/

[13] J. D. Heebl, E. M. Thomas, R. P. Penno, A. Grbic, Comprehensive Analysis and Measurement of Frequency-Tuned and Impedance-Tuned Wireless Non-Radiative Power-Transfer Systems, IEEE Antennas and Propagation Magazine 56 (5) (2014) 131–148. doi:10.1109/MAP.2014.6971924.
URL http://ieeexplore.ieee.org/document/6971924/

[14] T. Imura, H. Okabe, Y. Hori, Basic experimental study on helical antennas of wireless power transfer for Electric Vehicles by using magnetic resonant couplings, in: 2009 IEEE Vehicle Power and Propulsion Conference, IEEE, 2009, pp. 936–940. doi:10.1109/VPPC.2009.5289747.
URL http://ieeexplore.ieee.org/document/5289747/

[15] K. Colak, E. Asa, M. Bojarski, D. Czarkowski, O. C. Onar, A Novel Phase-Shift Control of Semibridgeless Active Rectifier for Wireless

19

Power Transfer, IEEE Transactions on Power Electronics 30 (11) (2015) 6288–6297. doi:10.1109/TPEL.2015.2430832.
URL http://ieeexplore.ieee.org/document/7105940/

[16] B. H. Choi, V. X. Thai, E. S. Lee, J. H. Kim, C. T. Rim, Dipole-Coil-Based Wide-Range Inductive Power Transfer Systems for Wireless Sensors, IEEE Transactions on Industrial Electronics 63 (5) (2016) 3158–3167. doi:10.1109/TIE.2016.2517061.
URL http://ieeexplore.ieee.org/document/7378949/

[17] W. Guenther, Antenna arrangement for inductive power transmission and use of the antenna arrangement (2009).

[18] G. A. Covic, J. T. Boys, Modern Trends in Inductive Power Transfer for Transportation Applications, IEEE Journal of Emerging and Selected Topics in Power Electronics 1 (1) (2013) 28–41. doi:10.1109/JESTPE.2013.2264473.
URL http://ieeexplore.ieee.org/document/6517868/

[19] A. Q. Cai, L. Siek, A 2-kW, 95% Efficiency Inductive Power Transfer System Using Gallium Nitride Gate Injection Transistors, IEEE Journal of Emerging and Selected Topics in Power Electronics 5 (1) (2017) 458–468. doi:10.1109/JESTPE.2016.2632743.
URL http://ieeexplore.ieee.org/document/7756384/

[20] K. A. Kalwar, M. Aamir, S. Mekhilef, Inductively coupled power transfer (ICPT) for electric vehicle charging – A review, Renewable and Sustainable Energy Reviews 47 (2015) 462–475. doi:10.1016/J.RSER.2015.03.040.
URL https://www.sciencedirect.com/science/article/pii/S1364032115001938

[21] C. Xia, R. Chen, Y. Liu, L. Liu, G. Chen, Inhibition of current harmonics in LCL/LCC wireless power transfer system, in: 2017 IEEE PELS Workshop on Emerging Technologies: Wireless Power Transfer, WoW 2017, Institute of Electrical and Electronics Engineers Inc., 2017. doi:10.1109/WoW.2017.7959390.

[22] M. Liu, M. Fu, C. Ma, Low-harmonic-contents and high-efficiency class e full-wave current-driven rectifier for megahertz wireless power transfer

systems, IEEE Transactions on Power Electronics 32 (2) (2017) 1198–1209. doi:10.1109/TPEL.2016.2551288.

[23] S. Luo, S. Li, H. Zhao, Reactive power comparison of four-coil, LCC and CLC compensation network for wireless power transfer, in: 2017 IEEE PELS Workshop on Emerging Technologies: Wireless Power Transfer, WoW 2017, Institute of Electrical and Electronics Engineers Inc., 2017, pp. 268–271. doi:10.1109/WoW.2017.7959407.

[24] Y. Li, R. Mai, M. Yang, Z. He, Cascaded multi-level inverter based IPT systems for high power applications, Journal of Power Electronics 15 (6) (2015) 1508–1516. doi:10.6113/JPE.2015.15.6.1508.

[25] Y. Li, R. Mai, L. Lu, Z. He, S. Liu, Harmonic elimination and power regulation based five-level inverter for supplying IPT systems, in: IEEE WoW 2015 - IEEE PELS Workshop on Emerging Technologies: Wireless Power, Proceedings, Institute of Electrical and Electronics Engineers Inc., 2015. doi:10.1109/WoW.2015.7132843.

[26] S. Sis, E. Orta, S. A. Sis, E. Orta, A Cross-Shape Coil Structure for Use in Wireless Power Applications, Energies 11 (5) (2018) 1094. doi:10.3390/en11051094.
URL http://www.mdpi.com/1996-1073/11/5/1094

[27] M. Budhia, G. Covic, J. Boys, A new IPT magnetic coupler for electric vehicle charging systems, in: IECON 2010 - 36th Annual Conference on IEEE Industrial Electronics Society, IEEE, 2010, pp. 2487–2492. doi:10.1109/IECON.2010.5675350.
URL http://ieeexplore.ieee.org/document/5675350/

[28] M. Budhia, J. T. Boys, G. A. Covic, C.-Y. Huang, Development of a Single-Sided Flux Magnetic Coupler for Electric Vehicle IPT Charging Systems, IEEE Transactions on Industrial Electronics 60 (1) (2013) 318–328. doi:10.1109/TIE.2011.2179274.
URL http://ieeexplore.ieee.org/document/6099605/

[29] T.-D. Nguyen, S. Li, W. Li, C. C. Mi, Feasibility study on bipolar pads for efficient wireless power chargers, in: 2014 IEEE Applied Power Electronics Conference and Exposition - APEC 2014, IEEE, 2014, pp. 1676–1682. doi:10.1109/APEC.2014.6803531.
URL http://ieeexplore.ieee.org/document/6803531/

[30] M. Alam, S. Mekhilef, H. Bassi, M. Rawa, Analysis of LC-LC2 Compensated Inductive Power Transfer for High Efficiency and Load Independent Voltage Gain, Energies 11 (11) (2018) 2883. doi:10.3390/en11112883.
URL http://www.mdpi.com/1996-1073/11/11/2883

[31] K. A. Kalwar, M. Aamir, S. Mekhilef, A design method for developing a high misalignment tolerant wireless charging system for electric vehicles, Measurement: Journal of the International Measurement Confederation 118 (2018) 237–245. doi:10.1016/j.measurement.2017.12.013.

[32] M. K. Uddin, S. Mekhilef, G. Ramasamy, Compact wireless IPT system using a modified voltage-fed multi-resonant class EF2inverter, Journal of Power Electronics 18 (1) (2018) 277–288. doi:10.6113/JPE.2018.18.1.277.

[33] Y. Shi, Y. Zhang, M. Shen, Y. Fan, C. Wang, M. Wang, Design of a novel receiving structure for wireless power transfer with the enhancement of magnetic coupling, AEU - International Journal of Electronics and Communications 95 (2018) 236–241. doi:10.1016/j.aeue.2018.08.033.

[34] D. A. Gonzalez, J. C. McCall, Design of Filters to Reduce Harmonic Distortion in Industrial Power Systems, IEEE Transactions on Industry Applications IA-23 (3) (1987) 504–511. doi:10.1109/TIA.1987.4504938.
URL http://ieeexplore.ieee.org/document/4504938/

[35] A. V. Oppenheim, A. S. Willsky, S. H. Nawab, Signals & Systems, (2nd ed.) Edition, Prentice-Hall, Inc., Upper Saddle River, NJ, USA, 1996.

[36] S. A. Sis, F. Kilic, S. Sezen, Multi sub-coil flux pipe couplers and their use in a misalignment-adaptive wireless power transfer system, Journal of Electromagnetic Waves and Applications 33 (14) (2019) 1890–1904. doi:10.1080/09205071.2019.1652117.
URL https://www.tandfonline.com/doi/full/10.1080/09205071.2019.1652117